metals

MDPI

Article

Improving Strength and Ductility of a Mg-3.7Al-1.8Ca-0.4Mn Alloy with Refined and Dispersed Al_2Ca Particles by Industrial-Scale ECAP Processing

Ce Wang [1], Aibin Ma [1,2,*], Jiapeng Sun [1], Xiaoru Zhuo [1], He Huang [1], Huan Liu [1,3,*], Zhenquan Yang [1] and Jinghua Jiang [1]

1 College of Mechanics and Materials, Hohai University, Nanjing 211100, China
2 Suqian Research Institute, Hohai University, Suqian 223800, China
3 Ocean and Coastal Engineering Research Institute, Hohai University, Nantong 226300, China
* Correspondence: aibin-ma@hhu.edu.cn (A.M.); liuhuanseu@hhu.edu.cn (H.L.); Tel.: +86-025-8378-7239 (A.M.)

Received: 24 June 2019; Accepted: 8 July 2019; Published: 9 July 2019

Abstract: Tailoring the morphology and distribution of the Al_2Ca second phase is important for improving mechanical properties of Al_2Ca-containing Mg-Al-Ca based alloys. This work employed the industrial-scale multi-pass rotary-die equal channel angular pressing (RD-ECAP) on an as-cast Mg-3.7Al-1.8Ca-0.4Mn (wt %) alloy and investigated its microstructure evolution and mechanical properties under three different processing parameters. The obtained results showed that RD-ECAP was effective for refining the microstructure and breaking the network-shaped Al_2Ca phase. With the increase of the ECAP number and decrease of the processing temperature, the average sizes of Al_2Ca particles decreased obviously, and the dispersion of the Al_2Ca phase became more uniform. In addition, more ECAP passes and lower processing temperature resulted in finer α-Mg grains. Tensile test results indicated that the 573 K-12p alloy with the finest and most dispersed Al_2Ca particles exhibited superior mechanical properties with tensile yield strength of 304 MPa, ultimate tensile strength of 354 MPa and elongation of 10.3%. The improved comprehensive mechanical performance could be attributed to refined DRX grains, nano-sized $Mg_{17}Al_{12}$ precipitates and dispersed Al_2Ca particles, where the refined and dispersed Al_2Ca particles played a more dominant role in strengthening the alloys.

Keywords: Mg-3.7Al-1.8Ca-0.4Mn alloy; Al_2Ca phase; equal channel angular pressing; refinement; mechanical properties

1. Introduction

Developing strong and ductile magnesium alloys has been one of the main research areas in the last twenty years, as they exhibit great potential in aerospace, military, new energy automobile, medical instrument and electronic applications [1–5]. High strength magnesium alloys with ultimate tensile strength higher than 400 MPa have already been successfully prepared with the addition of abundant rare-earth (RE) elements, owing to the intense second phase (precipitate) strengthening effect [6–8]. However, the RE addition impairs the lightweight advantage of magnesium alloys, and increased their cost as well, making them difficult to use for cost-sensitive industry applications [9–11]. Therefore, design and preparation of reinforced RE-free magnesium alloys have recently regained people's attention.

Mg-Al based (AZ series) alloys are one of the most commonly used commercial magnesium alloy series, whose strengthening precipitate is mainly $Mg_{17}Al_{12}$ phase [12–14]. $Mg_{17}Al_{12}$ possesses a

relatively low melting point (730 K) and tends to be softened above 473 K, thereby exhibiting a weak strengthening effect, especially at high temperatures [15,16]. In the last few years, the Mg-Al-Ca (-Mn) alloys, which were employed as typical heat-resistant casting magnesium alloys formerly, have been researched for high strength wrought Mg alloys. Ultrahigh strength characteristics involving tensile yield strength exceeding 400 MPa have already been obtained for high-Ca-content Mg-Al-Ca-Mn alloys [17–21]. However, excessive Ca addition intrinsically deteriorated the ductility of Mg alloys, whose elongations were always lower than 5%, even after remarkable grain refinement [17–20]. To balance the strength and ductility, Ca content should be decreased in these alloys.

With the increase of Ca content in Mg-Al-Ca alloys, $Mg_{17}Al_{12}$ phase turns into three laves phases in sequence, namely, Al_2Ca (C15), $(Mg,Al)_2Ca$ (C36) and Mg_2Ca (C14) phases, respectively [17]. Among these intermetallic compounds, Al_2Ca phase possesses the highest melting point, approximately 1352 K [22]. Studies of the first-principles calculation also proved that Al_2Ca phase exhibits the best thermal stability for the three laves phases [23]. Moreover, Al_2Ca phase could form with low or moderate Ca addition, which might facilitate a maximum combination of strength and ductility. So far, most Al_2Ca-containing magnesium alloys were prepared by hot extrusion, and they usually exhibited remarkably improved strength [24–26]. Although Al_2Ca network phases were crushed after extrusion, large particles remained and the broken particles were not uniformly distributed within a α-Mg matrix. As a consequence, local stress concentration was easy to generate at the junctions of brittle second phase particles and α-Mg matrix during a tensile test, resulting in nucleation and propagation of microcracks at an early time [19]. Therefore, it is essential to develop an effective method to refine Al_2Ca phases and increase their dispersibility, in order to improve the ductility of these high strength alloys.

Our previous studies have already shown that the multi-pass equal channel angler pressing (ECAP) is effective to refine large Al-Si particles, and network-shaped second phases in magnesium alloys [27–33]. As for Al_2Ca containing alloys, no attempt of ECAP processing has been reported. Therefore, in the present work, we prepared an Al_2Ca-dominated Mg-3.7Al-1.8Ca-0.4Mn (wt %) alloy first, and then systematically investigated its microstructural evolution and mechanical properties under an industrial-scale ECAP processing at three different processing parameters. By refining and dispersing Al_2Ca second phase particles, we successfully prepared a high strength and high ductility Al_2Ca-containing magnesium alloy block.

2. Materials and Methods

The raw materials for preparation of studied Mg-3.7Al-1.8Ca-0.4Mn (wt %) alloy were pure Mg, pure Al, Mg-30 wt % Ca and Mg-10 wt % Mn master alloys. The designed alloy was prepared by semi-continuous casting method, with an ingot diameter of 90 mm. Then large cuboid samples with dimension of 50 mm × 50 mm × 100 mm were cut from the center of the ingot for further industrial-scale ECAP. To explore the influence of processing parameters on refinement of Al_2Ca-containing alloys, three ECAP routes were proposed, i.e., 4 passes at 623 K, 12 passes at 623 K, and 12 passes at 573 K. The ECAP die employed was a self-design rotary-die (RD) with die angle of 90 ° and outer arc angle of 0°, which was described detailedly in our previous work [33]. Before ECAP, the sample was inserted in the die and both were heated and kept at a set temperature for 20 min within an induction heating furnace. Then multi-pass RD-ECAP were performed successively by an automatic control system without intermediate heating. This ECAP process is time-saving, and the total processing time for 12 passes was less than 15 min.

Metallographic specimens were then cut from the cast and ECAP specimens, mechanically grinded by #80, #400, #1000 and #2000 SiC abrasive papers, polished and etched with a 4 mL nitric acid and 96 mL ethanol mixed solution. Then, microstructure characterizations of the alloys were carried out by the X-ray diffractometer (XRD, Cu-Kα, Bruker D8, DISCOVER, Bruker Corporation, Karlsruhe, Germany), optical microscope (OM, Olympus BX51M, Olympus, Tokyo, Japan), and a scanning electron microscope (SEM, Sirion 200, FEI Company, Hillsboro, OR, USA) equipped with an X-ray energy dispersed spectrometer (EDS, Genesis 60S, FEI Company, Hillsboro, OR, USA). To further identify

various phases, observation of the transmission electron microscope (TEM, Tecnai G2, FEI Company, Hillsboro, OR, USA) was conducted. The TEM samples were prepared by mechanical grinding and ion thinning. To reveal the grain size distributions of ECAP alloys, the electron back-scatted diffraction (EBSD) analyses were conducted (SEM, Hitachi S-3400N, Hitachi, Tokyo, Japan). Moreover, the average particle sizes were measured by counting at least 100 particles in three SEM images through the Image-J software (Image 1.48, NationalInstitutes of Health, Bethesda, MD, USA). To evaluate the mechanical properties, tensile tests were performed via a CMT5105 electronic universal testing machine (MTS, Shenzhen, China) with a ram speed of 0.5 mm/min at room temperature. The dumbbell shaped specimens with gauge dimension of 7.5 mm × 2 mm × 2 mm were cut from the center section of ECAP samples with the loading direction parallel to the extrusion direction. For each processing situations, three tensile specimens were employed.

3. Results and Discussions

3.1. Microstructure of As-Cast Alloy

Figure 1 shows the XRD patterns of as-cast alloy and three ECAP alloys. Two phases, α-Mg and Al_2Ca phases, are indexed from the diffraction peaks for all alloys, which suggests no obvious phase transformation occurs during hot deformation. Since the Ca/Al ratio of this alloy is lower than 0.8, Al_2Ca phase becomes the main second phase [24]. Figure 2a,b show the optical and SEM micrographs of as-cast Mg-3.7Al-1.8Ca-0.4Mn alloy. Dendritic α-Mg grains and continuous-network interdendritic second phases (marked by A in Figure 2b) could be observed. Seen from the enlargement of the network phase shown in Figure 2c, it exhibits a lamellar shape, consistent with the morphology of a typical eutectic structure. The corresponding EDS result (Figure 2e) reveals high contents of Al and Ca elements, indicating they could have a Al_2Ca + α-Mg eutectic structure. Figure 3 shows the TEM image of the eutectic structure. Black and white stripes are arranged alternately. The index of the corresponding selected area electron diffraction (SAED) pattern of the black stripes (inset of Figure 3) further demonstrates the existence of Al_2Ca phase.

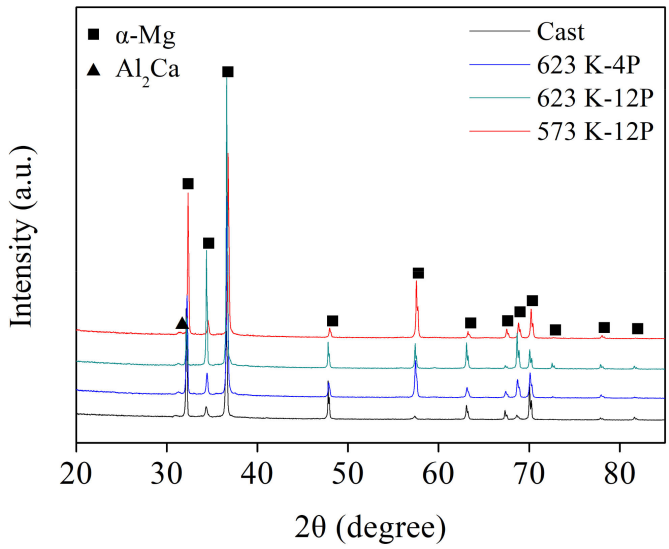

Figure 1. X-ray diffractometer (XRD) patterns of as-cast and ECAP-ed alloys.

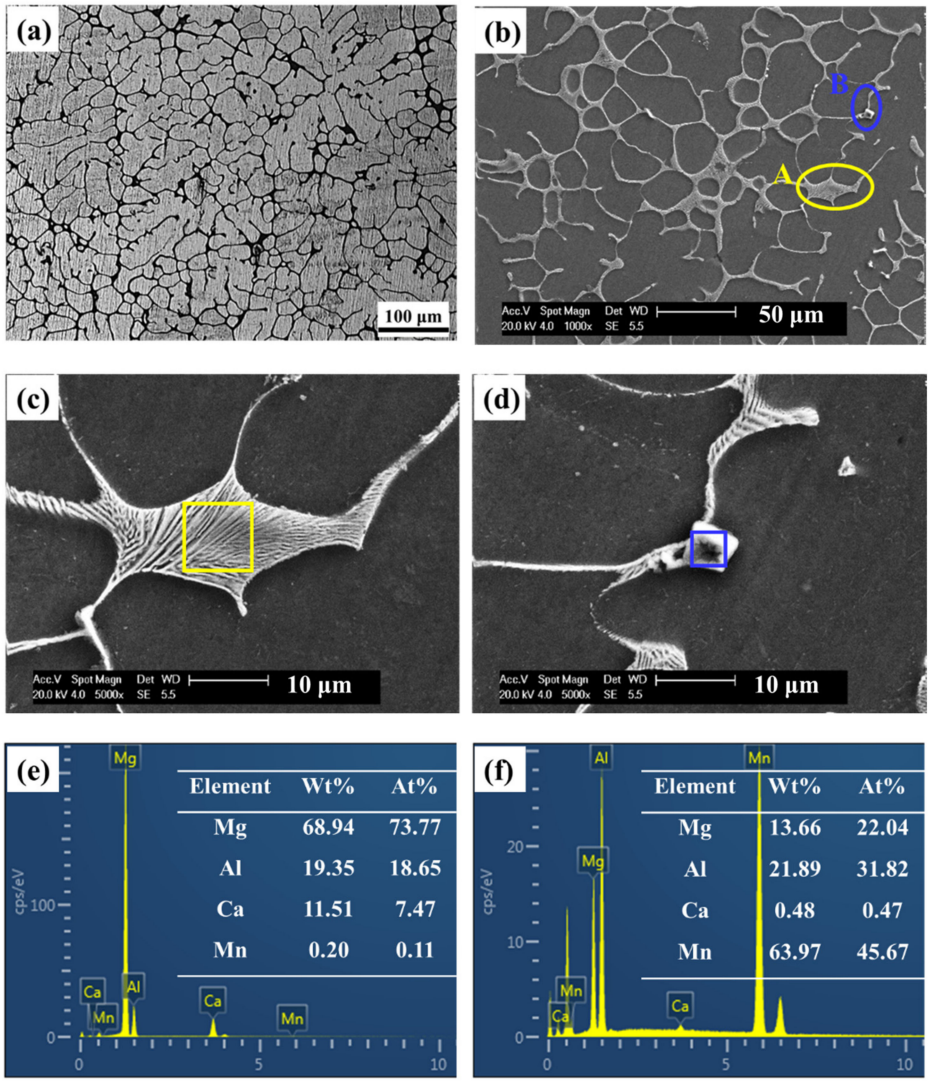

Figure 2. Microstructure of the as-cast alloy. (**a**) Optical image; (**b**,**c**,**d**) scanning electron microscope (SEM) images and enlargements of (**c**) the eutectic structure and (**d**) cubic particle; The corresponding EDS results of (**e**) the eutectic and (**f**) the particle.

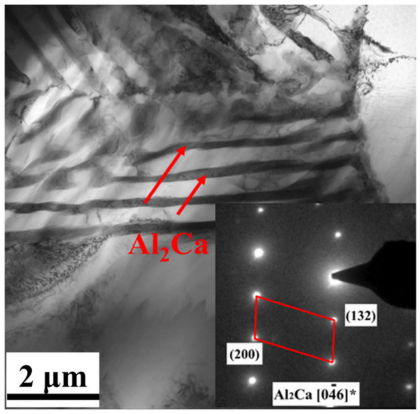

Figure 3. Transmission electron microscope (TEM) micrograph of the eutectic structure and the corresponding selected area electron diffraction (SAED) pattern of the black lamellar phases.

Moreover, some cubic particles (marked by B in Figure 2b) are observed near the eutectic network. EDS analysis on one particle (Figure 2d) was performed and the result (Figure 2f) suggested that it

contains much higher Mn and Al elements, which should be Al_8Mn_5 phase [19]. However, Al-Mn particles were not detected from the XRD patterns due to the fact that the content is extremely low.

3.2. Microstructure of ECAP Alloys

Figure 4 shows the SEM images of three Mg-3.7Al-1.8Ca-0.4Mn ECAP alloys processed at different temperatures and passes. Seen from the low-magnification images of Figure 4a,c,e, the continuous network eutectic structure became distorted after ECAP, and more ECAP numbers and a lower processing temperature resulted in a finer microstructure and narrower dendrite spacing. Moreover, as can be seen from the enlarged SEM images of Figure 4b,d,f, the distorted Al_2Ca dendritic phases were broken into ultrafine particles (with particle size lower than 1 μm). However, the average sizes of broken Al_2Ca particles are different in three ECAP alloys. High ECAP numbers refined the Al_2Ca particles from 0.6 μm to 0.5 μm for 623K-4p and 623K-12p alloys, while lower ECAP temperature was more effective to refine these particles, and the average size of Al_2Ca particles was approximately 0.3 μm in 573 K-12p alloy.

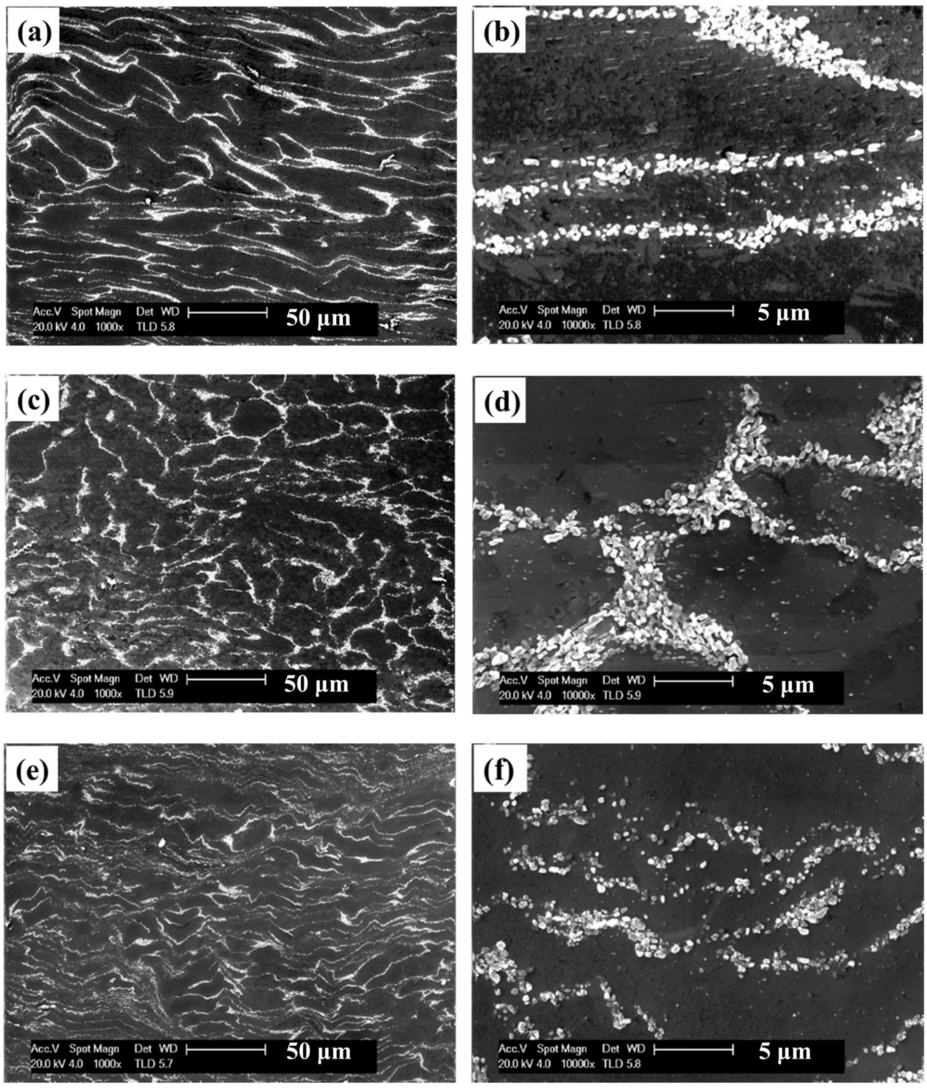

Figure 4. SEM images of ECAP alloys processed at (**a**,**b**) 623 K-4P, (**c**,**d**) 623 K-12P and (**e**,**f**) 573 K-12P with (**a**,**c**,**e**) low and (**b**,**d**,**f**) high magnifications.

To characterize the grain size evolution of studied alloy during ECAP at different processing parameters, Figure 5 shows the inverse pole figure maps and grain size distribution histograms of

ECAP alloys along the extrusion direction. The 623 K-4p alloy showed an uneven grain size distribution. Both coarse and fine grains were identified, suggesting an incomplete dynamic recrystallized (DRX) microstructure. After 12p ECAP at either 623 K or 573 K, homogeneous grain size distribution was observed (Figure 5c,d), indicating a high degree of DRX. Furthermore, Figure 6 shows the area fraction of DRX grains and un-DRX grains in three ECAP alloys. It is apparent that the fraction of DRX grains in two 12p alloys were much higher than the 4p alloy.

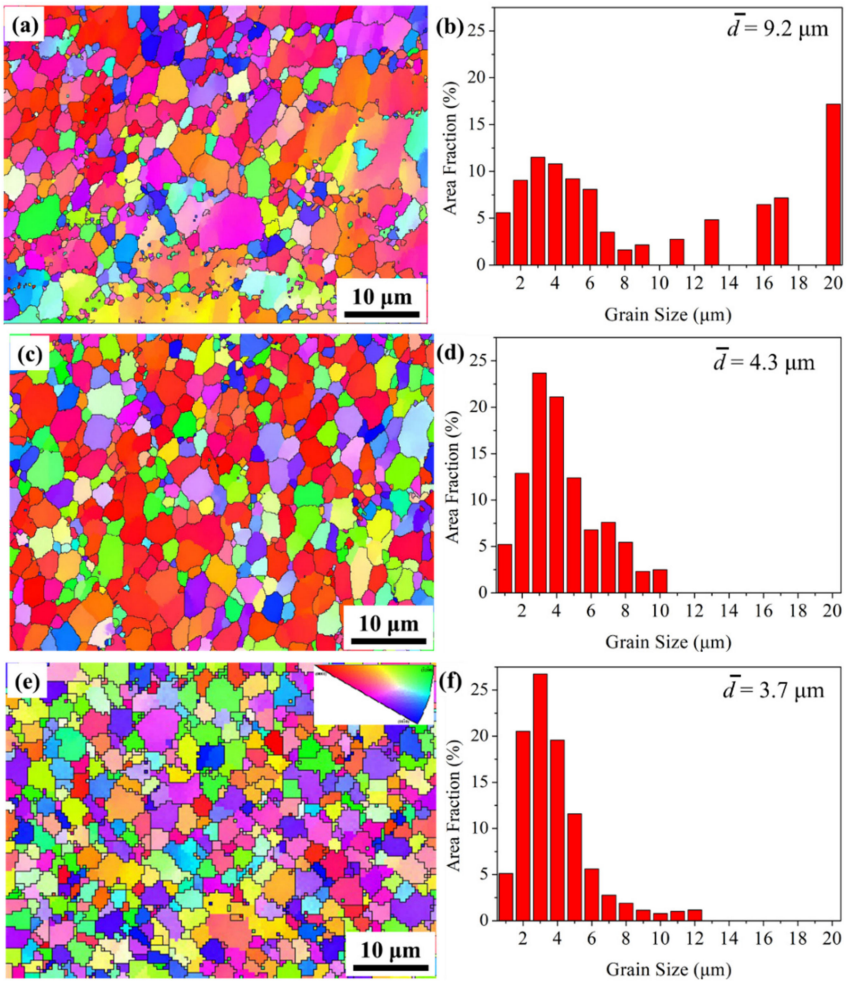

Figure 5. Electron back-scatted diffraction (EBSD) maps and its corresponding grains distributions of ECAP alloys processed from (**a**,**b**) 623 K-4P, (**c**,**d**) 623 K-12P and (**e**,**f**) 573 K-12P.

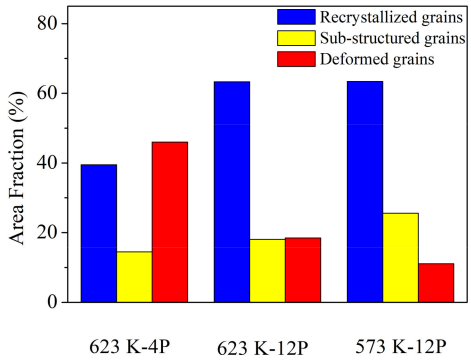

Figure 6. Area fraction of the recrystallized and un-recrystallized grains in three ECAP alloys.

Owing to the high DRX ratios, the average grain sizes of two 12p alloys were smaller than 4p alloy. The average grain sizes were estimated to be 9.2 μm, 4.3 μm and 3.7 μm for 623 K-4p, 623 K-12p and 573 K-12p alloys, respectively. It can be seen that higher ECAP numbers and lower processing temperature contributed to refinement and uniformity of α-Mg grains. Two factors resulted in finer grains for 573 K-12p alloy. For one thing, lower processing temperature could restrain the migrations of grain boundaries. For another, fine and dispersedly distributed Al_2Ca particles are more effective to hinder the growth of DRX grains. Figure 7 shows the TEM images of DRX regions in three ECAP alloys. High density of dislocations and sub-structures were observed in 623 K-4p alloy (Figure 7a). When the ECAP number increased to 12, the density of dislocations declined obviously, and the boundaries of DRX grains became distinct, either in 623 K and 573 K processed alloys. Overall, the grain sizes of DRX grains in these alloys are in good agreement with EBSD results.

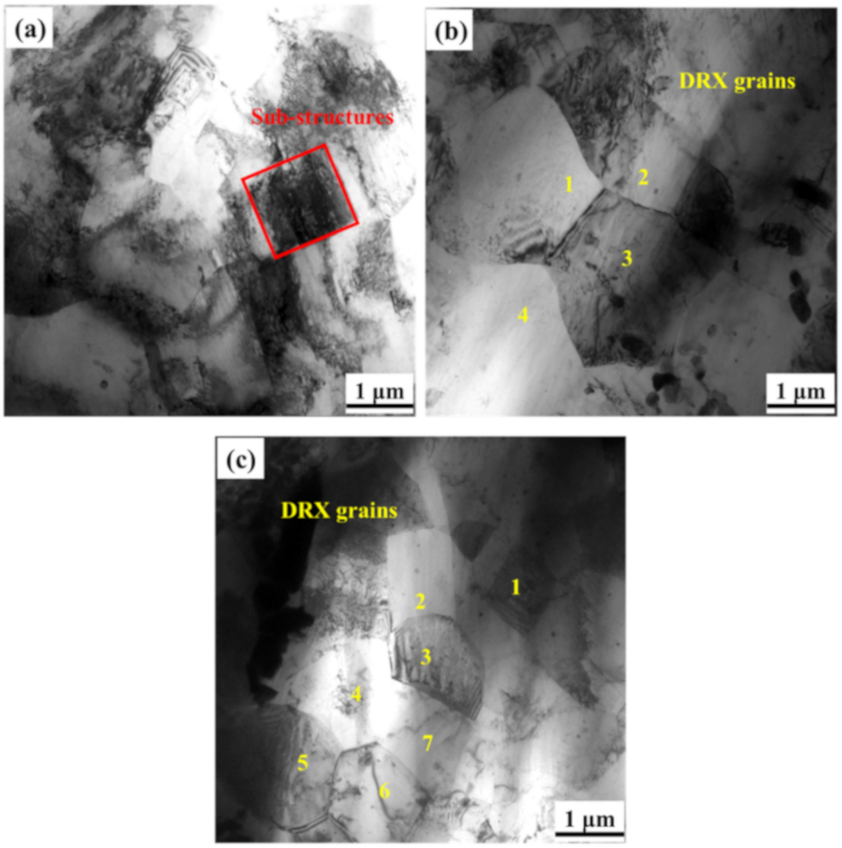

Figure 7. Ddynamic recrystallized (DRX) grains and sub-structured in (**a**) 623 K-4P, (**b**) 623 K-12P, (**c**) 573 K-12P alloys.

As can be seen from the Kernel Average Misorientation (KAM) maps shown in Figure 8, the distribution of dislocation density varied for three ECAP alloys (shown in green and yellow colors). It is shown in Figure 8a that fine DRX grains and coarse deformation grains were mixed in 623 K-4p alloy. Plenty of dislocations existed within coarse deformed grains, while fine DRX grains had little dislocations within, because the operation of DRX consumed dislocations. After increasing ECAP number to 12, more DRX fine grains and less deformation grains suggested a lower density of dislocations (Figure 8b). Moreover, compared with Figure 8b,c, it can be concluded that lower temperature processing led to stronger strain accumulation for ECAP alloys at the same pass (shown in green color).

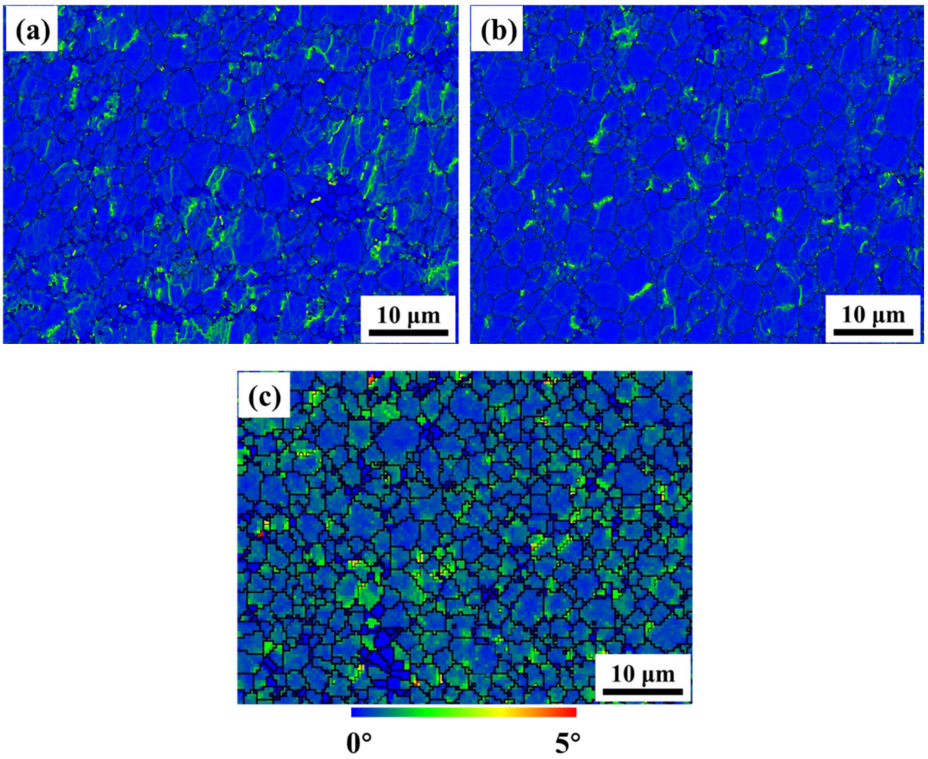

Figure 8. Kernel Average Misorientation (KAM) maps of alloys processed by (**a**) 623 K-4P, (**b**) 623 K-12P and (**c**) 573 K-12P.

Figure 9 shows the inverse pole figures of three ECAP alloys. A typical fiber texture (i.e., c-axes perpendicular to the extrusion direction) was formed for 623 K-4p alloy, and its maximum texture intensity was 2.40 (Figure 9a). Increasing processing number to 623 K, the orientations (c-axes) of grains exhibited a tendency to be parallel to extrusion direction, and the maximum intensity was 4.89 (Figure 9b). With the decrease of processing temperature to 573 K, the maximum texture intensity declined to 2.80. Similar texture evolutions have also been found in other recrystallized Mg-RE and AZ series magnesium alloys [34,35].

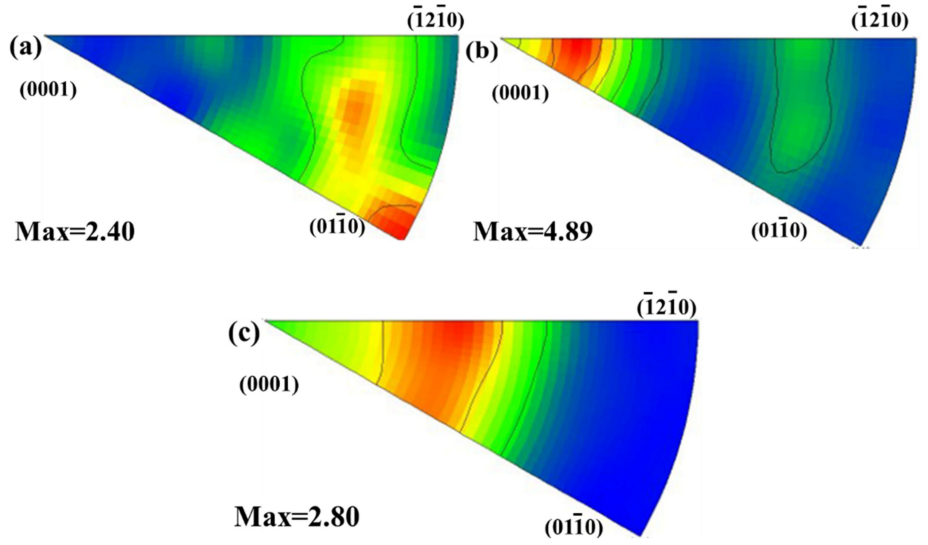

Figure 9. Inverse pole figures of ECAP alloys processed from (**a**) 623 K-4P, (**b**) 623 K-12P and (**c**) 573 K-12P.

Figure 10 exhibits the TEM observation of Al_2Ca second phase in three deformed alloys. In early ECAP passes at 623 K, lamellar Al_2Ca eutectic phase was partially broken into fine particles, as can be seen from the Al_2Ca laths and particles shown in Figure 10a,b, respectively. Since Al_2Ca is a brittle phase, its refining mechanism is more like a mechanical crushing process. Therefore, the crush of Al_2Ca eutectic phase was incomplete and uneven owing to the low deformation strains at low ECAP pass. When the ECAP number was increased to 12, the Al_2Ca phase broke thoroughly into submicron particles (Figure 10b,c), though they were still aggregated.

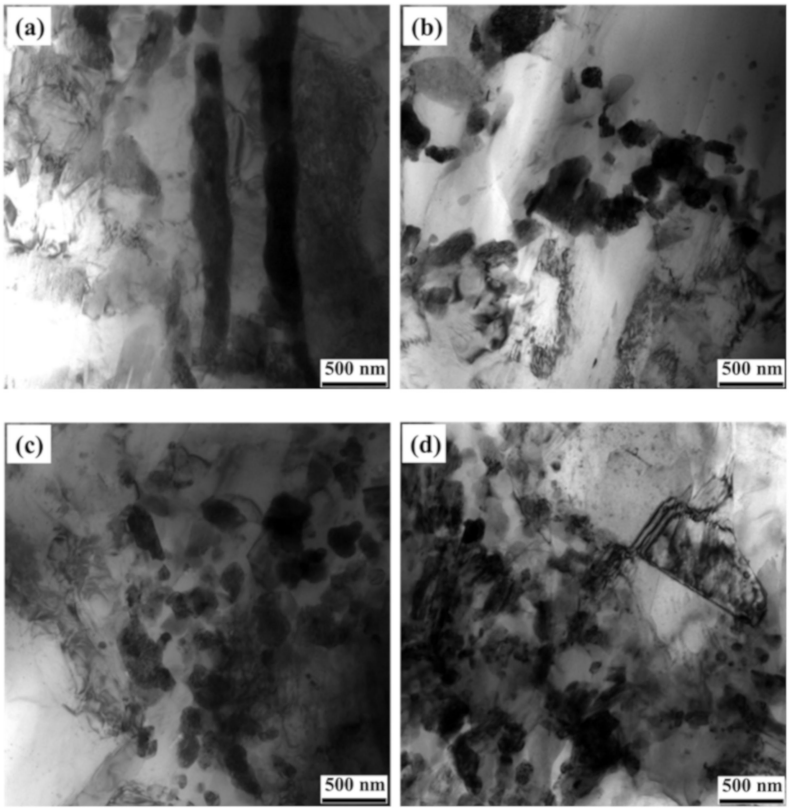

Figure 10. TEM images of Al_2Ca phase particles in (**a**,**b**) 623 K-4P, (**c**) 623 K-12P and (**d**) 573 K-12P alloys.

Furthermore, TEM observations demonstrated that abundant nano-sized precipitates were observed within un-DRX α-Mg grains (including sub-grains) of all ECAP alloys (Figure 11), while the density of precipitates was relatively low in DRX grains. These precipitates were dynamically precipitated during hot deformation, which was commonly observed in Mg-Al-Ca based alloys. Most of the precipitates had a spherical shape (marked by yellow arrows), and a few exhibited rod shapes (red arrows). Seen from Figure 11a, the diameters of these spherical precipitates were around 5–15 nm in 623 K-4p alloy. With increased ECAP numbers, the density of precipitates increased for 623 K-12p alloy, and both rod-like and spherical precipitates were observed. The rod-like precipitates are usually larger than spherical particles, exhibiting a diameter of 20–30 nm and a length of 30–60 nm. After 12 passes of ECAP at 573 K, precipitates with diameter of 10–20 nm were also detected (Figure 11c), and the precipitation density was the highest for three deformed alloys. Furthermore, Figure 11d shows the corresponding SAED patterns of the precipitates. The diffraction patterns exhibit near-ring characteristic, and index of the diffraction rings demonstrates that the precipitates are $Mg_{17}Al_{12}$ phases. The $Mg_{17}Al_{12}$ precipitates are usually reported in AZ91 alloys [36]. As for Mg-Al-Ca alloys, Al_2Ca phase served as the main precipitates during hot deformation or aging in most cases [24], and precipitation of $Mg_{17}Al_{12}$ particles was barely reported. Taking into account the alloy composition and microstructure of this studied alloy, most Ca elements were concentrated within the eutectic phases,

and Al elements were more inclined to be enriched in some grains, which caused the precipitation of $Mg_{17}Al_{12}$ phases under the interaction of heat and strain during multi-pass ECAP.

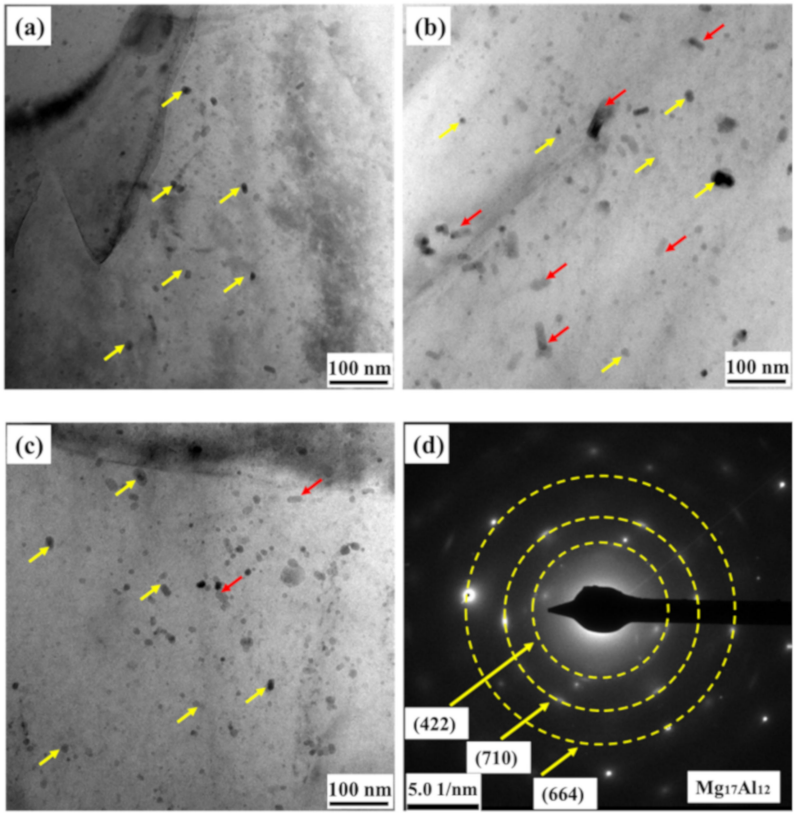

Figure 11. TEM micrographs of the precipitates in (**a**) 623 K-4P, (**b**) 623 K-12P, and (**c**)573 K-12P alloys, as well as (**d**) the corresponding SAED patterns of the precipitates.

3.3. Microstructure of ECAP Alloys

Figure 12 shows the tensile mechanical properties of as-cast and ECAP alloys. The as-cast alloy possessed low mechanical properties with tensile yield strength (TYS) of 70 MPa, ultimate tensile strength (UTS) of 161 MPa and poor ductility (elongation of 5.1%). After the ECAP process, all samples exhibited a remarkable improvement in both strength and ductility. Generally, an increase in the ECAP numbers improved the strength and ductility simultaneously, while decreases in ECAP temperatures further enhanced the alloy, but impaired the ductility slightly. The 573 K-12p alloy showed the highest strength, with TYS of 304 MPa and UTS of 354 MPa, together with a moderate ductility. In addition, by comparing with other commercial Mg alloys and Mg-RE based alloys prepared by ECAP (Figure 12c) [27–32,37–39], this 573 K-12p alloy exhibits a relatively high specific yield strength, which is comparable to those Mg-RE ECAP alloys with high RE contents. Overall, this non-RE low-alloying ECAP alloy with refined and dispersed Al_2Ca particles exhibits great potential as high performance magnesium alloys.

Figure 13 shows the SEM fractograph of as-cast and ECAP alloys after tensile tests. Seen from Figure 13a, many laminated cleavage steps appear on the fracture surface of the as-cast alloy, suggesting a brittle fracture. Owing to the large eutectic structures at grain boundaries, microcracks tend to be formed around the eutectic, which leads to early break and poor ductility of the as-cast alloy. After ECAP, a few dimples and laminated cleavage steps are observed on fracture surface of 623 K-4p alloy (Figure 13b), indicating a mixed fracture mechanism. As for two 12p alloys (Figure 13c,d), although the fracture surfaces become fine and flat, some cleavage steps still exist.

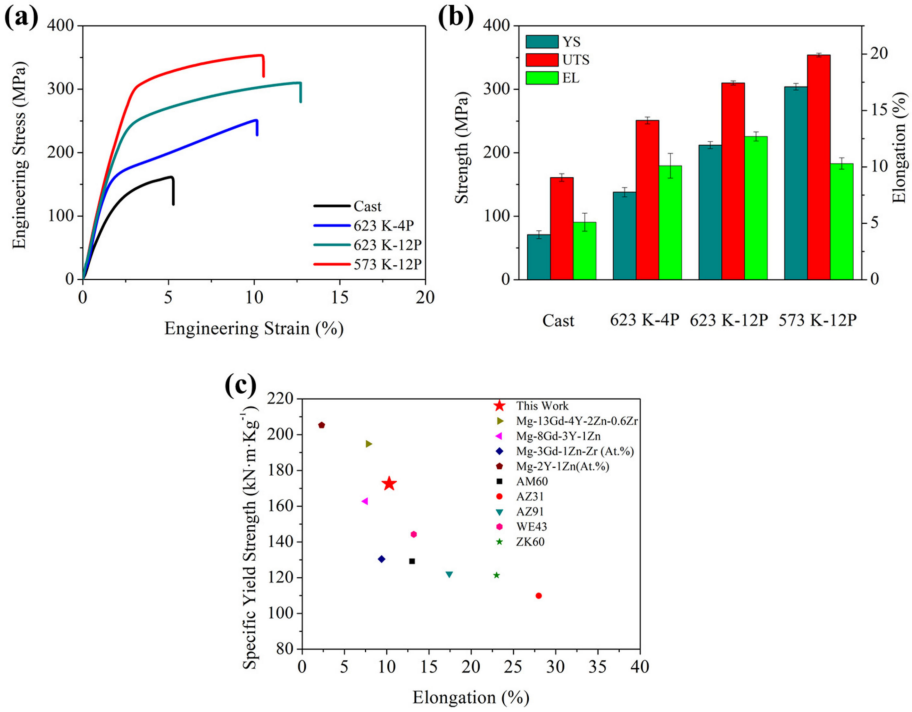

Figure 12. Mechanical properties of Mg-Al-Ca-Mn alloys. (**a**) Typical tensile curves of as-cast and ECAP alloys; (**b**) The summary of yield strength (YS), ultimate tensile strength (UTS) and elongation of various alloys; (**c**) Comparison of specific yield strength and elongation between this work and other high performance ECAP Mg alloys [27–32,37–39].

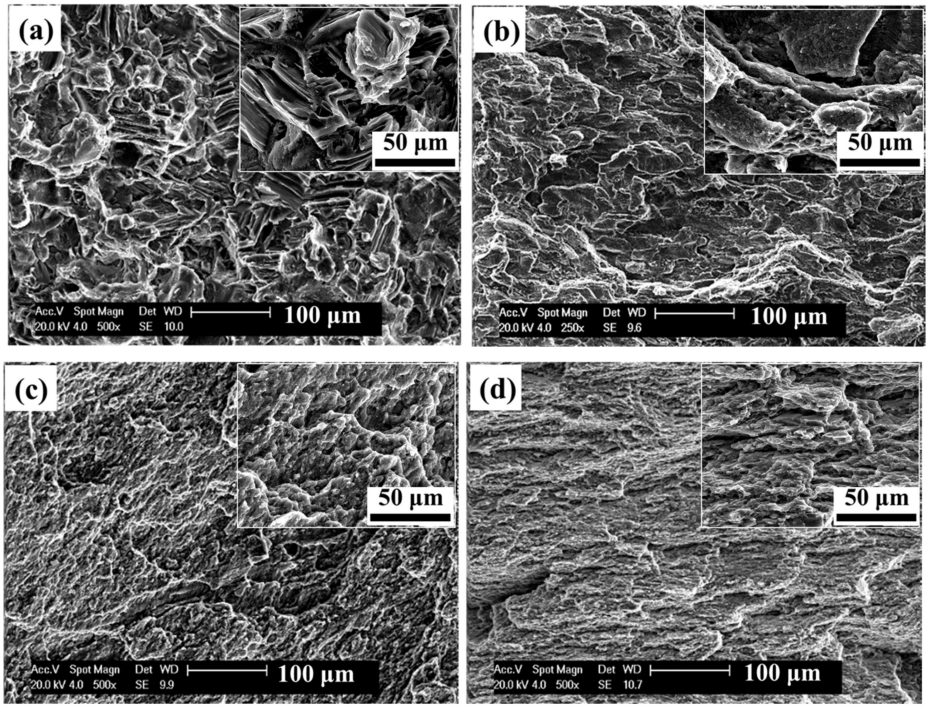

Figure 13. SEM images of fracture surfaces of (**a**) As-cast, (**b**) 623 K-4P, (**c**) 623 K-12P and (**d**) 573 K-12P alloys. Insets of the images are the corresponding enlarged micrographs.

3.4. Influence of Al_2Ca Size and Distribution on Mechanical Properties

Based on above tensile results, it can be confirmed that multi-pass ECAP is beneficial for improving the mechanical properties of an Al_2Ca-containing alloy. Considering the microstructural evolutions,

the improved strength of ECAP alloys could be mainly ascribed to three factors, i.e., refined DRX grains, dynamically precipitated $Mg_{17}Al_{12}$ precipitates, and dispersed Al_2Ca particles. To quantitatively describe the contributions of various strengthening factors, Table 1 lists the characteristic parameters of DRX grains and second phase particles.

Table 1. Microstructural characteristics of ECAP-ed alloys.

Microstructural Characteristics	623 K-4P	623 K-12P	573 K-12P
Grain (μm)	9.2 ± 1.9	4.3 ± 1.5	3.7 ± 1.2
Al_2Ca (μm)	0.6 ± 0.2	0.5 ± 0.2	0.3 ± 0.1
Ribbonlike Al_2Ca arm spacing (μm)	17 ± 4	11 ± 2	8 ± 2
$Mg_{17}Al_{12}$ (nm)	12 ± 4	22 ± 7	14 ± 6
$Mg_{17}Al_{12}$ volume fraction (%)	2.5%	6.7%	6.1%

The contribution of fine grain strengthening could be estimated from the Hall-Petch equation:

$$\sigma_y = \sigma_0 + kd^{-0.5}, \quad (1)$$

where σ_y is yield strength, σ_0 is material constants, k is Hall-Petch slope and d is grain size. The value of k was employed as 170 MPa·μm$^{1/2}$ on the basis of average grains in this work [40]. Accordingly, the contribution of grain refinement strengthening on tensile yield strength could be estimated to be 55 MPa, 97 MPa and 105 MPa for 623 K-4p, 623 K-12p, and 573 K-12p alloys, respectively.

In case of $Mg_{17}Al_{12}$ nano-particles precipitated at grain internal, they could pin dislocation movement and strengthen the alloy by Orowan strengthening mechanism [41]. The increment of YS associated with $Mg_{17}Al_{12}$ particles have already been given in an early report [41], and the equation is shown in Equation (2).

$$\Delta\sigma_{Orowan} = \beta \frac{0.4u_m b}{\pi\left(d\sqrt{\pi/4f_v} - 1\right)} \frac{\ln(d/b)}{\sqrt{1-v_m}}, \quad (2)$$

where β is constant (1.25), μ_m is shear modulus (16.5 GPa), b is Burgers vector (0.32 nm), d is the average size of $Mg_{17}Al_{12}$, f_v is the volume fraction of $Mg_{17}Al_{12}$, and ν_m is Poisson ratio (0.35). Moreover, is should be noticed from above TEM observations that the nano-sized $Mg_{17}Al_{12}$ particles were most dynamically precipitated in the un-DRX grains, and they were seldom seen in DRX grains, which has also been reported in other Mg-Al-Ca-Mn alloys [19]. Therefore, we assumed that the Orowan strengthening mechanism caused by $Mg_{17}Al_{12}$ precipitates is only activated in un-DRX grains, and it could be calculated by the following equation:

$$\Delta\sigma_{Mg17Al12} = (1 - f_{DRX})\Delta\sigma_{Orowan}, \quad (3)$$

where f_{DRX} is the volume fraction of DRX grains showed in Figure 6.

As long as the strengthening caused by grain refinement and $Mg_{17}Al_{12}$ precipitates was estimated, the rest of strengthening effect should be caused by the Al_2Ca second phase strengthening, and it is calculated by Equation (4),

$$\Delta\sigma_{Al_2Ca} = \sigma_{YS} - \sigma_{Cast} - \sigma_{Hall-Petch} - \sigma_{Mg17Al12}, \quad (4)$$

where σ_{YS} is the tested tensile yield strength of ECAP alloys, and σ_{Cast} is the tested tensile yield strength of cast alloy.

Figure 14a displays the quantitative contributions of grain refinement, dynamic precipitated $Mg_{17}Al_{12}$ precipitates and dispersed Al_2Ca second phase particles, to TYS values of three ECAP alloys. It is apparent that for 623 K-4P and 12p alloys, fine grain strengthening plays a more important role than other two strengthening factors. With the dispersion of Al_2Ca phase in 573 K-12p alloy, the strengthening contribution of the Al_2Ca phase exceeds the other two factors. To intuitively describe

the strengthening effect of a dispersed Al_2Ca second phase, Figure 14b shows the relationship between $\Delta\sigma_{Al2Ca}$ and the distance of ribbonlike Al_2Ca arm spacing [42]. It is obvious that with the decrease of Al_2Ca arm spacing, the contribution of the Al_2Ca phase increases remarkably. Therefore, to further improve the mechanical properties of Al_2Ca containing Mg-Al-Ca-Mn alloys, additional effort should be focused on the refining and dispersion of Al_2Ca second phase particles.

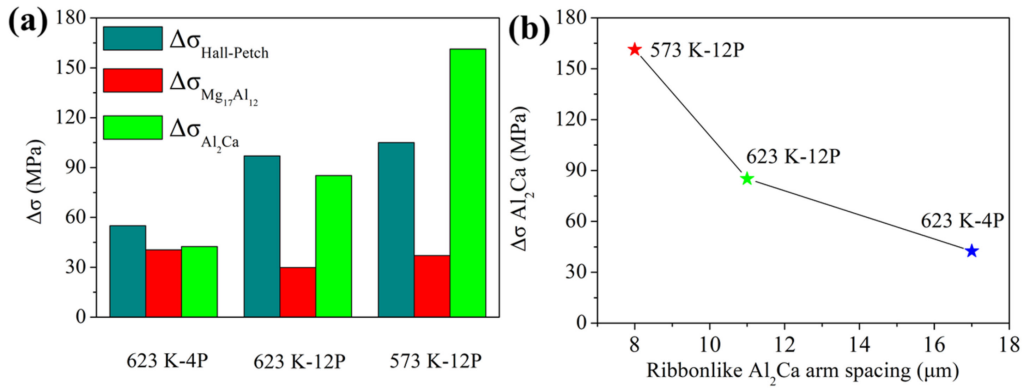

Figure 14. (**a**) The contributions of various strengthening factors to tensile yield strength of ECAP alloys. (**b**) The relationship between the ribbonlike Al_2Ca arm spacing and the contribution of Al_2Ca particles to tensile yield strength of ECAP alloys.

4. Conclusions

The microstructure evolutions and mechanical properties of a Mg-3.5Al-1.7Ca-0.4Mn (wt %) alloy during ECAP at different processing numbers and temperatures were systematically investigated. The main conclusions can be drawn as follows:

(1) The microstructure of as-cast Mg-3.5Al-1.7Ca-0.4Mn (wt %) alloy was composed of interdendritic α-Mg grains, network Al_2Ca phase and a few Al_8Mn_5 particles. During multi-pass ECAP, the Al_2Ca network phase was gradually broken into ultrafine particles. More ECAP passes and lower processing temperature resulted in finer sizes and a more dispersed distribution of Al_2Ca particles, as well as finer α-Mg grains.

(2) Multi-pass ECAP simultaneously enhanced the tensile strength and ductility of Mg-3.5Al-1.8Ca-0.4Mn alloy. The 573 K-12p processed alloy exhibited superior mechanical properties with a tensile yield strength of 304 MPa, ultimate tensile strength of 354 MPa and elongation of 10.3%. The improved comprehensive mechanical performance could be attributed to refined DRX grains, nano-sized $Mg_{17}Al_{12}$ precipitates and dispersed Al_2Ca particles. Moreover, quantitative contribution analysis suggested that the refined and dispersedly distributed Al_2Ca particles played a dominant role in strengthening the Al_2Ca containing alloys.

Author Contributions: A.M., H.L. and J.J. designed the project and guided the research; C.W., J.S. and H.L. prepared the manuscript; C.W., H.H. and Z.Y. performed the experiment and analyzed the data; X.Z., H.H. and C.W. prepared the figures; A.M., H.L. and J.J. reviewed the manuscript.

Funding: The authors are grateful to the financial aid from the Natural Science Foundation of Jiangsu Province of China (BK20160869), the National Natural Science Foundation of China (51774109 and 51501039), the Fundamental Research Funds for the Central Universities (2018B48414), the Key Research and Development Project of Jiangsu Province of China (BE2017148), and the Nantong Science and Technology Project (JC2018109).

Data Availability: The raw/processed data required to reproduce these findings cannot be shared at this time as the data also forms part of an ongoing study.

Conflicts of Interest: The authors declare no conflict of interest.

References

1. Mordike, B.L.; Ebert, T. Magnesium: Properties-applications-potential. *Mater. Sci. Eng. A* **2001**, *302*, 37–45. [CrossRef]
2. Yamashita, A.; Horita, Z.; Langdon, T.G. Improving the mechanical properties of magnesium and a magnesium alloy through severe plastic deformation. *Mater. Sci. Eng. A* **2001**, *300*, 142–147. [CrossRef]
3. Song, M.S.; Zeng, R.C.; Ding, Y.F.; Li, R.W.; Easton, M.; Cole, I.; Birbilis, N.; Chen, X.B. Recent advances in biodegradation controls over Mg alloys for bone fracture management: A review. *J. Mater. Sci. Technol.* **2019**, *35*, 535–544. [CrossRef]
4. Wang, B.J.; Wang, S.D.; Xu, D.K.; Han, E.H. Recent progress in the research about fatigue behavior of Mg alloys in air and aqueous medium: A review. *J. Mater. Sci. Technol.* **2017**, *33*, 1075–1086. [CrossRef]
5. Liu, H.; Huang, H.; Sun, J.P.; Wang, C.; Bai, J.; Ma, A.B.; Chen, X.H. Microstructure and mechanical properties of Mg-RE-TM cast alloys containing long period stacking ordered phases: A review. *Acta. Metall. Sin. Engl.* **2019**, *32*, 269–285. [CrossRef]
6. Wang, X.J.; Xu, D.K.; Wu, R.Z.; Chen, X.B.; Peng, Q.M.; Jin, L.; Xin, Y.C.; Zhang, Z.Q.; Liu, Y.; Chen, X.H.; et al. What is going on in magnesium alloys? *J. Mater. Sci. Technol.* **2018**, *34*, 245–247. [CrossRef]
7. Liu, H.; Huang, H.; Wang, C.; Ju, J.; Sun, J.; Wu, Y.; Jiang, J.; Ma, A. Comparative study of two aging treatments on microstructure and mechanical properties of an ultra-fine grained Mg-10Y-6Gd-1.5Zn-0.5Zr alloy. *Metals* **2018**, *8*, 658. [CrossRef]
8. Liu, H.; Huang, H.; Wang, C.; Sun, J.; Bai, J.; Xue, F.; Ma, A.; Chen, X.B. Recent advances in LPSO-containing wrought magnesium alloys: Relationships between processing, microstructure, and mechanical properties. *JOM* **2019**, 1–14. [CrossRef]
9. Zhang, J.H.; Liu, S.J.; Wu, R.Z.; Hou, L.G.; Zhang, M.L. Recent developments in high-strength Mg-RE-based alloys: Focusing on Mg-Gd and Mg-Y systems. *J. Magnes. Alloy* **2018**, *6*, 277–291. [CrossRef]
10. Pan, H.C.; Qin, G.W.; Huang, Y.M.; Ren, Y.P.; Sha, X.C.; Han, X.D.; Liu, Z.Q.; Li, C.F.; Wu, X.L.; Chen, H.W.; et al. Development of low-alloyed and rare-earth-free magnesium alloys having ultra-high strength. *Acta Mater.* **2018**, *149*, 350–363. [CrossRef]
11. Fu, L.; Le, Q.C.; Tang, Y.; Sun, J.Y.; Jia, Y.H.; Song, Z.T. Effect of Ca and RE additions on microstructures and tensile properties of AZ31 alloys. *Mater. Res. Express* **2018**, *5*, 056521. [CrossRef]
12. Cheng, C.; Lan, Q.; Wang, A.; Le, Q.; Yang, F.; Li, X. Effect of Ca additions on ignition temperature and multi-Stage oxidation behavior of AZ80. *Metals* **2018**, *8*, 766. [CrossRef]
13. Kim, S.H.; Lee, J.U.; Kim, Y.J.; Moon, B.G.; You, B.S.; Kim, H.S.; Parka, S.H. Improvement in extrudability and mechanical properties of AZ91 alloy through extrusion with artificial cooling. *Mater. Sci. Eng. A* **2017**, *703*, 1–8. [CrossRef]
14. Kang, J.W.; Sun, X.F.; Deng, K.K.; Xu, F.J.; Zhang, X.; Bai, Y. High strength Mg-9Al serial alloy processed by slow extrusion. *Mater. Sci. Eng. A* **2017**, *697*, 211–216. [CrossRef]
15. Han, L.; Hu, H.; Northwood, D.O. Effect of Ca additions on microstructure and microhardness of an as-cast Mg–5.0 wt. % Al alloy. *Mater. Lett.* **2008**, *62*, 381–384. [CrossRef]
16. Kondori, B.; Mahmudi, R. Effect of Ca additions on the microstructure and creep properties of a cast Mg-Al-Mn magnesium alloy. *Mater. Sci. Eng. A* **2017**, *700*, 438–447. [CrossRef]
17. Xu, S.W.; Oh-ishi, K.; Kamado, S.; Uchida, F.; Homma, T.; Hono, K. High-strength extruded Mg-Al-Ca-Mn alloy. *Scr. Mater.* **2011**, *65*, 269–272. [CrossRef]
18. Li, Z.T.; Zhang, X.D.; Zheng, M.Y.; Qiao, X.G.; Wu, K.; Xu, C.; Kamado, S. Effect of Ca/Al ratio on microstructure and mechanical properties of Mg-Al-Ca-Mn alloys. *Mater. Sci. Eng. A* **2017**, *682*, 423–432. [CrossRef]
19. Li, Z.T.; Qiao, X.G.; Xu, C.; Kamado, S.; Zheng, M.Y.; Luo, A.A. Ultrahigh strength Mg-Al-Ca-Mn extrusion alloys with various aluminum contents. *J. Alloys Compd.* **2019**, *792*, 130–141. [CrossRef]
20. Khorasani, F.; Emamy, M.; Malekan, M.; Mirzadeh, H.; Pourbahari, B.; Krajnák, T.; Minárik, P. Enhancement of the microstructure and elevated temperature mechanical properties of as-cast Mg-Al_2Ca-Mg_2Ca in-situ composite by hot extrusion. *Mater. Charact.* **2019**, *147*, 155–164. [CrossRef]
21. Wang, C.; Ma, A.; Sun, J.; Liu, H.; Huang, H.; Yang, Z.; Jiang, J. Effect of ECAP process on as-cast and as-homogenized Mg-Al-Ca-Mn alloys with different Mg_2Ca morphologies. *J. Alloys Compd.* **2019**, *793*, 259–270. [CrossRef]
22. Watanabe, H.; Yamaguchi, M.; Takigawa, Y.; Higashi, K. Mechanical properties of Mg-Al-Ca alloy processed by hot extrusion. *Mater. Sci. Eng. A* **2007**, *454*, 384–388. [CrossRef]

23. Zhou, D.W.; Liu, J.S.; Peng, P.; Chen, L.; Hu, Y.J. A first-principles study on the structural stability of Al_2Ca Al_4Ca and Mg_2Ca phases. *Mater. Lett.* **2008**, *62*, 206–210. [CrossRef]
24. Jiang, Z.T.; Jiang, B.; Yang, H.; Yang, Q.S.; Dai, J.H.; Pan, F.S. Influence of the Al_2Ca phase on microstructure and mechanical properties of Mg-Al-Ca alloys. *J. Alloys Compd.* **2015**, *647*, 357–363. [CrossRef]
25. Su, K.; Deng, K.K.; Xu, F.J.; Nie, K.B.; Zhang, L.; Zhang, X.; Li, W.J. Effect of extrusion temperature on the microstructure and mechanical properties of Mg-5Al-2Ca alloy. *Acta. Metall. Sin. Engl.* **2015**, *28*, 1015–1023. [CrossRef]
26. Homma, T.; Hirawatari, S.; Sunohara, H.; Kamado, S. Room and elevated temperature mechanical properties in the as-extruded Mg-Al-Ca-Mn alloys. *Mater. Sci. Eng. A* **2012**, *539*, 163–169. [CrossRef]
27. Jin, L.; Lin, D.L.; Mao, D.L.; Zeng, X.Q.; Ding, W.J. Mechanical properties and microstructure of AZ31 Mg alloy processed by two-step equal channel angular extrusion. *Mater. Lett.* **2005**, *59*, 2267–2270. [CrossRef]
28. Sun, J.P.; Yang, Z.Q.; Han, J.; Liu, H.; Song, D.; Jiang, J.H.; Ma, A.B. High strength and ductility AZ91 magnesium alloy with multi-heterogenous microstructures prepared by high-temperature ECAP and short-time aging. *Mater. Sci. Eng. A* **2018**, *734*, 485–490. [CrossRef]
29. Garces, G.; Pérez, P.; Barea, R.; Medina, J.; Stark, A.; Schell, N.; Adeva, P. Increase in the mechanical strength of Mg-8Gd-3Y-1Zn alloy containing long-period stacking ordered phases using equal channel angular pressing processing. *Metals* **2019**, *9*, 221. [CrossRef]
30. Chen, B.; Lin, D.L.; Zeng, X.Q.; Lu, C. Microstructure and mechanical properties of ultrafine grained $Mg_{97}Y_2Zn_1$ alloy processed by equal channel angular pressing. *J. Alloys Compd.* **2007**, *440*, 94–100. [CrossRef]
31. Zhang, J.S.; Zhang, W.B.; Bian, L.P.; Cheng, W.L.; Niu, X.F.; Xu, C.X.; Wu, S.J. Study of Mg-Gd-Zn-Zr alloys with long period stacking ordered structures. *Mater. Sci. Eng. A* **2013**, *585*, 268–276. [CrossRef]
32. Martynenko, N.S.; Lukyanova, E.A.; Serebryany, V.N.; Gorshenkov, M.V.; Shchetinin, I.V.; Raab, G.I.; Dobatkin, S.V.; Estrin, Y. Increasing strength and ductility of magnesium alloy WE43 by equal-channel angular pressing. *Mater. Sci. Eng. A* **2018**, *712*, 625–629. [CrossRef]
33. Ma, A.B.; Nishida, Y.; Suzuki, K.; Shigematsu, I.; Saito, N. Characteristics of plastic deformation by rotary-die equal-channel angular pressing. *Scr. Mater.* **2005**, *52*, 433–437. [CrossRef]
34. Jin, L.; Lin, D.L.; Mao, D.L.; Zeng, X.Q.; Ding, W.J. An electron back-scattered diffraction study on the microstructure evolution of AZ31 Mg alloy during equal channel angular extrusion. *J. Alloys Compd.* **2006**, *426*, 148–154. [CrossRef]
35. Rong, W.; Zhang, Y.; Wu, Y.J.; Chen, Y.L.; Sun, M.; Chen, J.; Peng, L.M. The role of bimodal-grained structure in strengthening tensile strength and decreasing yield asymmetry of Mg-Gd-Zn-Zr alloys. *Mater. Sci. Eng. A* **2019**, *740*, 262–273. [CrossRef]
36. Yang, Z.; Ma, A.; Liu, H.; Sun, J.; Song, D.; Wang, C.; Yuan, Y.; Jiang, J. Multimodal microstructure and mechanical properties of AZ91 Mg alloy prepared by equal channel angular pressing plus aging. *Metals* **2018**, *8*, 763. [CrossRef]
37. Li, B.; Teng, B.G.; Chen, G.X. Microstructure evolution and mechanical properties of Mg-Gd-Y-Zn-Zr alloy during equal channel angular pressing. *Mater. Sci. Eng. A* **2019**, *744*, 396–405. [CrossRef]
38. Akbaripanah, F.; Saniee, F.F.; Mahmudi, R.; Kim, H.K. Microstructural homogeneity, texture, tensile and shear behavior of AM60 magnesium alloy produced by extrusion and equal channel angular pressing. *Mater. Des.* **2013**, *43*, 31–39. [CrossRef]
39. Dumitru, F.D.; Cobos, O.F.H.; Cabrera, J.M. ZK60 alloy processed by ECAP: Microstructural, physical and mechanical characterization. *Mater. Sci. Eng. A* **2014**, *594*, 32–39. [CrossRef]
40. Yu, H.H.; Xin, Y.C.; Wang, M.Y.; Liu, Q. Hall-petch relationship in Mg alloys: A review. *J. Mater. Sci. Technol.* **2018**, *34*, 248–256. [CrossRef]
41. Sun, X.F.; Wang, C.J.; Deng, K.K.; Nie, K.B.; Zhang, X.C.; Xiao, X.Y. High strength SiCp/AZ91 composite assisted by dynamic precipitated $Mg_{17}Al_{12}$ phase. *J. Alloys Compd.* **2018**, *732*, 328–335. [CrossRef]
42. Yamasaki, M.; Hashimoto, K.; Hagihara, K.; Kawamura, Y. Effect of multimodal microstructure evolution on mechanical properties of Mg-Zn-Y extruded alloy. *Acta Mater.* **2011**, *59*, 3646–3658. [CrossRef]